Available online at www.sciencedirect.com
SCIENCE DIRECT®
Journal of Solid State Chemistry 176 (2003) 250–258
JOURNAL OF SOLID STATE CHEMISTRY
http://elsevier.com/locate/jssc

Effect of heat treatment on the structure of L-Ta_2O_5: a study by XRPD and HRTEM methods

Charlotta Askeljung, Bengt-Olov Marinder, and Margareta Sundberg*

Department of Inorganic Chemistry, Arrhenius Laboratory, Stockholm University, Stockholm SE-106 91, Sweden

Received 24 April 2003; received in revised form 15 July 2003; accepted 25 July 2003

Abstract

The effect of heat treatment on the structure of L-Ta_2O_5 has been studied by X-ray powder diffraction and high-resolution transmission electron microscopy, complemented by density measurements. Two stable low-temperature forms of L-Ta_2O_5 were found: one below about 1000°C with a b^* multiplicity of $m \approx 13.5$ and the other at 1350°C with $m = 11$. The former modification was disordered, containing defects and twins, while the latter seemed to be more ordered. At intermediate temperatures, ordered and disordered mixtures of L-Ta_2O_5 slabs with m values in the range $m = 11-14$ were seen. A new model of a structure of L-Ta_2O_5 ($m = 11$) is proposed. The model can be described as an ordered intergrowth of slabs of α-U_3O_8 and β-U_3O_8 types. The α-U_3O_8 slabs are wider and contain somewhat larger three-sided tunnels that appear to be more suitable for interstitial Ta atoms than the β-U_3O_8 slabs. The density measurements confirm that additional Ta atoms are present in the structure.

Keywords: L-Ta_2O_5; Structure; Multiplicity; X-ray diffraction; HRTEM; Density; Disorder; Intergrowth structure; α-U_3O_8; β-U_3O_8

1. Introduction

The low-temperature variety of tantalum pentoxide, L-Ta_2O_5, exhibits a sluggishly reversible phase transition to a high-temperature modification at about 1360°C. It is therefore difficult to grow single crystals of the low-temperature form by conventional high-temperature techniques [1–4]. The X-ray powder pattern of L-Ta_2O_5 contains strong subcell lines and a number of weak extra lines. Lehovec showed [5] that the stronger lines in the X-ray pattern from an amorphous Ta_2O_5 sample annealed for 8 h at 1100°C could be indexed by using a unit cell with $a = 6.20$, $b = 3.66$ and $c = 3.89$ Å. From cited density values ($\rho \approx 8.02-8.27$ g/cm^3) Lehovec concluded that the subcell contained one formula unit of Ta_2O_5. Compiling orthorhombic unit-cell dimensions proposed by various authors and comparing them with those of the subcell above, he noted the occurrence of unit cells with 2-, 12- and 19-fold increased b-axis. The diversity of published density values of L-Ta_2O_5, 8.18–8.41 g/cm^3, is pointed out in Ref. [6]. In order to account for the extra lines, Frevel and Rinn [7] and Terao [8] had to use monoclinic unit cells. The density of L-Ta_2O_5 according to Terao is 8.90 ± 0.01 g/cm^3. Moser [9] tried to classify L-Ta_2O_5 modifications by noting the position of one characteristic line, the so-called C line, occurring at a 2θ value of about 26° (Cu$K\alpha$ radiation). The position of this reflection has turned out to be strongly dependent on sample preparation, thermal treatment and impurity content.

Difficulties in obtaining single crystals of L-Ta_2O_5 necessitated attempts to introduce certain amounts of other oxides in order to stabilize the L-Ta_2O_5 structure. The oxides added contained three-, four-, and six-valent cations. In particular, phases in the system Ta_2WO_8–Ta_2O_5 have been studied [10–19], and the L-Ta_2O_5-related crystal structures of $Ta_{22}W_4O_{67}$, $Ta_{30}W_2O_{81}$ and $Ta_{38}WO_{98}$ determined from X-ray single-crystal data [14–16]. Very small single-crystals of L-Ta_2O_5 itself could eventually be prepared and a structure determination carried out [20]. These four structures have multiplicities $m = 13, 8, 19$, and 11, where $m = b_0^*/b^*$ and b_0^* corresponds to the lattice cell dimension given by Lehovec [5].

A building-block scheme was developed, based on Andresen's structure for U_3O_8 [21], consisting of edge-

*Corresponding author. Fax: +46-8-15-21-87.
E-mail address: marsu@inorg.su.se (M. Sundberg).

0022-4596/$ - see front matter © 2003 Elsevier Inc. All rights reserved.
doi:10.1016/j.jssc.2003.07.003

sharing pentagonal bipyramids with octahedra between the chains, whereby an ideal structure could be predicted for this type of compound. The oxygen:metal ratio of this structure (2.667) can be reduced to a certain extent by "folding" of the straight chains. Further reduction of the ratio is obtained by introducing oxygen vacancies in so-called distortion planes. Fig. 1a shows an idealized crystal structure of L-Ta_2O_5 ($m = 11$), suggested by Stephenson and Roth [20], that contains 22 metal and 58 oxygen atoms. The real structure, according to these authors, has oxygen vacancies in the metal plane, thus reducing the number of oxygens to 55 per unit cell.

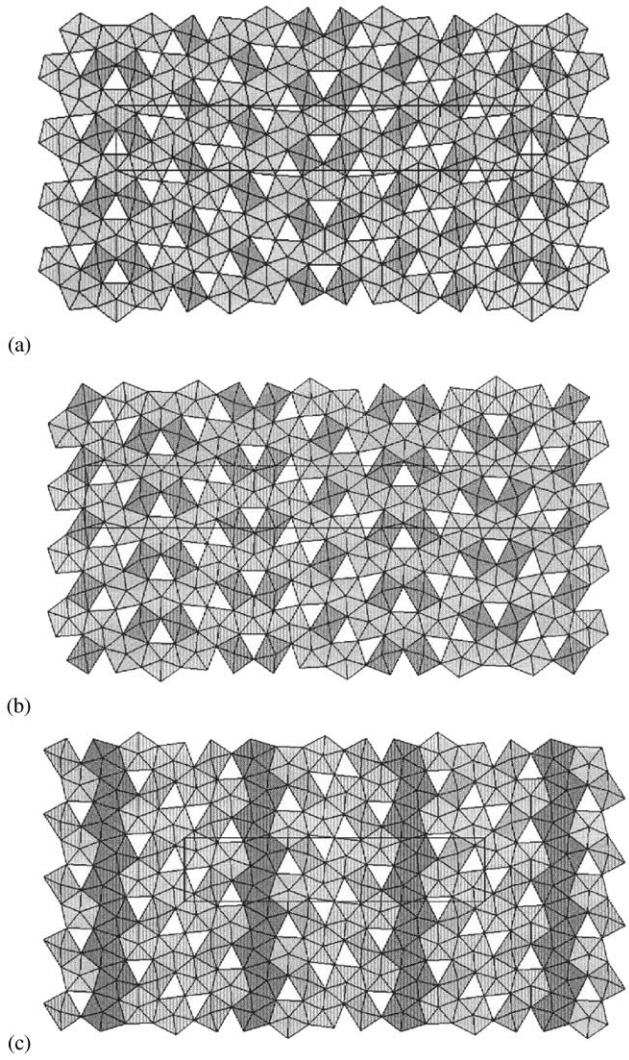

Fig. 1. (a) The idealized crystal structure of L-Ta_2O_5 ($m = 11$) given in Ref. [20]. It is a β-U_3O_8(subcell)-type structure twinned at (010) and (020) with the actual composition Ta_2O_5. A further reduction of the O:Ta ratio is accomplished through oxygen vacancies in the metal plane. (b) The crystal structure of $Ta_{22}W_4O_{67}$ composed of β-U_3O_8 (subcell)-type elements of two different widths twinned at (010). Apical oxygen vacancies are assumed to satisfy the stoichiometry. (c) The crystal structure of $Ta_{74}W_6O_{203}$ composed of α-U_3O_8- and β-U_3O_8 (subcell)-type structures. Apical oxygen vacancies are assumed to satisfy the stoichiometry.

For pure Ta_2O_5 the conclusion has been reached [3,10] that there exist two low-temperature polymorphic phases. In as-received Ta_2O_5 and below about 1000°C a structure with $m = 14$ occurs, and at higher temperatures ($\approx$1350°C) one with $m = 11$. At intermediate temperatures ordered or partially ordered mixtures of the two phases occur in equilibrium with each other [3]. The former phase, with 14 subcell units, has also been observed in as-received Ta_2O_5 by high-resolution transmission electron microscopy (HRTEM) [22]. A single-crystal X-ray structure determination of Ta_2O_5 with $m = 12$, prepared by a transport reaction at about 800°C, has also been reported [23].

In 1992, Schmid et al. published a study of the L-Ta_2O_5–$Ta_{22}W_4O_{67}$ system using X-ray powder diffraction and transmission electron microscopy techniques [24]. They concluded that this range could be looked upon as an incommensurately modulated solid solution $(1–x)Ta_2O_5 \cdot xWO_3$, $0 \leqslant x \leqslant 0.267$, with a linearly composition-dependent primary modulation wave vector $\mathbf{q} = q \cdot \mathbf{b}^*$. The corresponding parent structure is supposed to be a slightly orthorhombically distorted, oxygen-deficient α-UO_3-type structure with $a \approx 6.20$, $b \approx 3.66$ and $c \approx 3.89$ Å, cf. Ref. [5]. For pure L-Ta_2O_5 heated at 1350°C the authors found $q = 0.635$, as compared to the theoretical value 7/11 or 0.6363… for a commensurate phase. The structures of $Ta_{22}W_4O_{67}$ ($x = 0.267$) and $Ta_{74}W_6O_{203}$ ($x = 0.140$), with 13- and 8-fold subcell units, respectively, have been refined as composite modulated structures from single-crystal studies with synchrotron radiation [25,26]. These structures are shown in Figs. 1b and c. Some apical oxygen vacancies are assumed to satisfy the stoichiometry. A structure of an L-Ta_2O_5 type phase in the TiO_2–Ta_2O_5 system, deduced from HRTEM images, has been described [27] as an ordered intergrowth of α-U_3O_8 and β-U_3O_8 structure types. Some of the images indicated presence of interstitial metal atoms. A relation between q and the multiplicity m based on the so-called C-line [9] is given in Ref. [28].

We may conclude that reported multiplicities of L-Ta_2O_5 ($m = 11$, 12 and 14) appear to vary with the synthesis, especially the annealing of the oxide. We also note a certain spread in the observed densities, as shown above and elsewhere in the literature. This information together with the observation that interstitial metal atoms may occur in the L-Ta_2O_5 type phase in the TiO_2–Ta_2O_5 system gave us the impetus to investigate L-Ta_2O_5 with a well-known thermal pre-history. Thus samples of L-Ta_2O_5, as received and heated at various temperatures for various periods of time, were investigated by X-ray powder diffraction and HRTEM techniques complemented by density measurements.

2. Experimental

The Ta_2O_5 powder used in this study was obtained from Strem Chemicals. This reagent is reported as containing 99.9% tantalum(V) oxide. Batches of 10–12 g were heated for various lengths of time in a platinum crucible as listed in Table 1. The samples were removed from the furnace and allowed to cool in the crucible. Smaller amounts of samples, however, were contained in unsealed platinum tubes and quenched from the actual calcination temperature as shown in Table 1. The purity of the starting material (sample E1) and the sample E8.23 (annealed at 1340°C for 588 h) was investigated by energy-dispersive X-ray spectroscopy in a JEOL 820 scanning electron microscope (SEM) equipped with a LINK system. The EDS spectra showed only peaks from tantalum. All samples were investigated by X-ray powder diffraction, using a Guinier–Hägg focusing camera with strictly monochromatized Cu$K\alpha_1$ radiation and with LaB_6 as internal θ standard (JCPDS-ICDD 34-427, $a = 4.15690$ Å). The powder photographs were evaluated with an automatic scanner system, and the unit-cell parameters were refined by least-squares techniques.

Density measurements, using helium displacement technique, were made in AccuPyc 1330 standard 10, 1 and 0.1 cm^3 Pycnometers from Micromeritics on batches of about 10, 2 and 0.2 g, respectively of Ta_2O_5. The instruments were checked by determining the densities of dried and ground NaCl, KCl and $Pb(NO_3)_2$. The densities obtained were found to be 1–2% lower than theoretical.

Electron-microscope specimens were prepared by crushing a small amount of the Ta_2O_5 sample under *n*-butanol in an agate mortar. A drop of the resultant suspension was allowed to dry on a copper grid coated with a holey carbon film. The electron microscopy studies were made on 10–15 fragments from each of the preparations in Table 1 (E1–E8.23). A large number of selected-area electron diffraction (ED) patterns were taken in different [*h*0*l*] orientations in the JEOL 2000FX-II transmission electron microscope, operated at 200 kV, which was equipped with a double-tilt, side-entry goniometer stage with tilt angles of $\pm 45°$. The HRTEM studies of thin crystals were made in the TEM-microscope, JEOL JEM-3010 (double-tilt $\pm$ 10–20°, side-entry goniometer stage) operated at 300 kV. Crystallographic image processing by the computer program system CRISP [29] was applied to a couple of HRTEM images taken of crystallites from the sample E8.23 in order to obtain more accurate tantalum atom positions. The structure models are produced with ATOMS by Shape Software.

3. Results

3.1. X-ray powder diffraction and density measurements

The strong reflections in the Guinier photographs were indexed using the orthorhombic parent unit cell with $a \approx 6.20$, $b \approx 3.66$ and $c \approx 3.89$ Å suggested by Lehovec [5]. The four-index notation

$$\mathbf{d}^*_{h\,k\,l\,n} = h\mathbf{a}^* + k\mathbf{b}^*_0 + l\mathbf{c}^* + n\mathbf{q}$$

used by Schmid et al. [24] was also used in the present study to index all the reflections. Here $\mathbf{a}^*$, $\mathbf{b}^*_0$ and $\mathbf{c}^*$ correspond to the reciprocal lattice cell dimensions of the parent structure, and $\mathbf{q} = q\cdot\mathbf{b}^*_0$ is a modulation wave vector. The data were subjected to a least-squares refinement out to about $2\theta = 75°$ for Cu$K\alpha_1$. The results are shown in Figs. 2a–e. The length of the *a*-axis decreases with increasing temperature of preparation (the 1350°C sample is an exception which may be due to the vicinity of the transition temperature to H-Ta_2O_5). The b_0- and *c*-axis, on the other hand, are

Table 1
Some experimental and derived results from L-Ta_2O_5

Sample	Heat treatment		V_{sub} (Å^3)	d_{obs}	Z_{sub}	q	$m = 1/(2-3q)$	$m = b^*_0/s^*$ from ED	Remarks
	Temp. (°C)	Time (h)							
E1	—	—	88.43(5)	8.65(2)	1.042(3)	0.6411(5)	13.0(3)	13.2	As received
E2	550	100	88.60(7)	8.64(1)	1.043(2)	0.6420(8)	13.5(5)	13.2	
E3	700	100	88.42(5)	8.62(1)	1.039(2)	0.6421(6)	13.6(4)	13.0	
E4	850	72	88.44(5)	8.61(1)	1.038(2)	0.6418(6)	13.4(4)	13.5	
E5	1000	72	88.42(6)	8.68(1)	1.046(2)	0.6417(5)	13.4(3)	13.5	
E6	1150	50	88.38(5)	8.72(2)	1.050(3)	0.6401(5)	12.5(3)	12.8	
E6.2	1150	96	88.41(6)	8.72(2)	1.051(4)	0.6402(5)	12.6(3)	13.1	From E6
E8	1300	24	88.38(4)	8.75(1)	1.054(2)	0.6402(3)	12.6(2)	12.2	
E8.2	1300	96	88.33(4)	8.75(1)	1.053(2)	0.6398(4)	12.4(2)	12.3	From E8
E8.21	550	160	88.37(4)	8.76(1)	1.055(2)	0.6396(3)	12.3(2)	12.4	From E8.2[a]
E8.22	1350	45	88.34(4)	8.76(1)	1.052(2)	0.6369(4)	11.2(2)	11.0	From E8.2[a]
E8.23	1340	588	88.35(4)	8.79(1)	1.058(2)	0.6370(3)	11.2(1)	10.9	From E8.2[a]

[a] In unsealed Pt-tubes and quenched from indicated temperature.

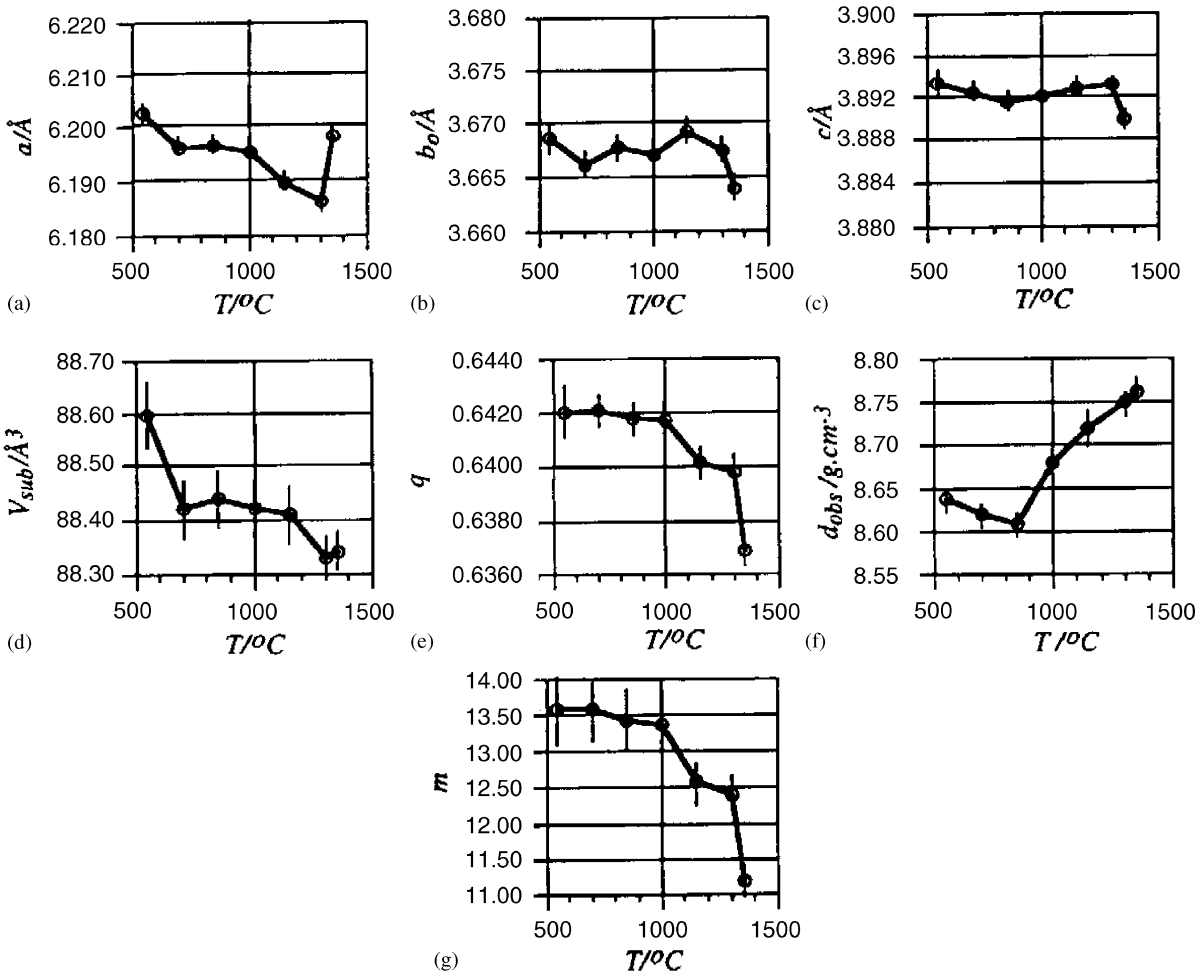

Fig. 2. Plots of data versus preparation temperature for L-Ta_2O_5. (a)–(d) Refined unit-cell dimensions, (e) q values obtained from refined XRPD-data, (f) observed density values, d_{obs}, and (g) multiplicity values $m = 1/(2-3q)$.

fairly constant. The subcell volumes and the q values decrease with increasing temperature of preparation (Figs. 2d and e). The density d_{obs} (Fig. 2f) first shows a slight decrease and then an increase. The multiplicity m, related to q as $m = 1/(2-3q)$ [28] shows a decrease with increasing temperature of preparation (Fig. 2g). Some further details of observed subcell volumes V_{sub}, densities d_{obs} and calculated numbers of formula units of Ta_2O_5, Z_{sub}, as well as q and m values are given in Table 1. Observed and calculated 2θ values for one of the samples (E8.2) are given in Table 2.

3.2. Electron microscopy studies

Electron microscopy studies of the starting material (E1) showed that the as-received Ta_2O_5 powder consisted to a large part of amorphous and badly crystallized fragments. The ED patterns of the latter crystallites showed severe streaking of the subcell reflections along b^*, and the multiplicity value as shown below could only be calculated from two of the recorded patterns. The amorphous fragments, on the other hand, seemed to crystallize when heated in the electron beam. The diffuse halos observed in the ED pattern from one fragment seemed to change into diffuse rings after a few minutes' exposure to the beam. Our results are similar to those previously reported on the crystallization of thin amorphous tantalum oxide films [30,31].

The ED patterns taken from well-ordered crystallites in the [001], [10−1] and [102] directions contained information about the multiplicity. The pattern in Fig. 3a ([001] zone) shows a pseudo-hexagonal arrangement of strong reflections that originate from the orthorhombic L-Ta_2O_5 subcell suggested by Lehovec [5]. In the three ED patterns (Figs. 3a–c) there are rows of superstructure spots, which are grouped in clusters around the subcell reflections and run parallel to b^*. This is even better seen in Fig. 3d, which shows an enlarged part of the $[-1k0]$ line in Fig. 3a. By measuring the

Table 2
Indexed X-ray powder pattern of L-Ta_2O_5 heated at 1300°C for 96 h. A four-index notation $(h,k,l,n) = h\mathbf{a}^* + k\mathbf{b}_0^* + l\mathbf{c}^* + n\mathbf{q}$ has been used, where $\mathbf{a}^*$, $\mathbf{b}_0^*$ and $\mathbf{c}^*$ are the cell vectors of a reciprocal lattice of a substructure of Lehovec-type with $a = 6.1862(7)$, $b_0 = 3.6674(4)$ and $c = 3.8932(5)$ Å ($\mathbf{q} = q\mathbf{b}_0^*$ with $q = 0.6396(3)$)

$2\theta_{obs}$	I_{obs}	d_{obs}	h	k	l	n	$\Delta(2\theta)$
16.769	2.32	5.283	1	1	0	−1	0.019
17.465	0.92	5.074	0	2	0	−2	0.059
22.819	79.44	3.894	0	0	1	0	0.000
26.552	6.96	3.354	1	1	0	−3	0.001
28.245	100.00	3.157	1	1	0	0	−0.015
28.459	7.68	3.134	1	1	1	−1	0.017
28.843	64.82	3.093	2	0	0	0	0.019
			0	2	1	−2	−0.006
30.027	2.34	2.974	1	3	0	−3	0.014
31.184	1.73	2.866	0	0	0	2	0.012
32.864	2.81	2.723	2	0	0	−1	0.006
33.884	5.26	2.643	2	2	0	−2	0.011
35.292	6.87	2.541	1	1	1	−3	0.009
36.631	82.29	2.451	1	1	1	0	0.004
37.099	54.57	2.421	2	0	1	0	0.023
			2	2	1	−3	−0.032
38.040	4.23	2.364	1	3	1	−3	0.006
40.391	1.03	2.231	2	0	1	−1	0.009
42.967	2.25	2.103	1	1	0	1	0.009
			2	0	0	2	−0.001
44.431	4.33	2.037	3	1	0	−2	0.022
44.548	1.84	2.032	2	2	0	−1	0.014
44.797	5.10	2.022	3	1	0	−1	0.015
44.949	3.05	2.015	1	3	0	−2	0.009
45.228	2.07	2.003	3	3	0	−4	−0.019
46.627	29.95	1.946	0	0	2	0	0.013
			0	2	2	−3	−0.033
49.194	4.67	1.851	2	0	1	2	−0.003
49.676	34.76	1.834	0	2	0	0	0.000
50.529	5.68	1.805	3	1	1	−2	0.030
50.730	22.71	1.798	3	1	0	0	0.003
50.990	2.09	1.790	1	3	1	−2	0.005
51.278	1.60	1.780	3	3	1	−4	0.017
51.822	7.19	1.763	3	3	0	−3	0.001
54.468	2.90	1.683	1	1	2	−3	0.020
55.390	79.62	1.657	0	2	1	0	0.059
			1	1	2	0	−0.019
55.759	22.06	1.647	2	0	2	0	0.024
			2	2	2	−3	−0.017
56.316	22.54	1.632	3	1	1	0	0.009
57.333	6.74	1.606	3	3	1	−3	0.006
58.442	16.81	1.578	2	2	0	0	−0.009
58.877	1.80	1.567	2	2	2	−2	0.021
59.302	1.71	1.557	1	1	0	2	0.013
59.745	8.11	1.547	4	0	0	0	0.038
			4	2	0	−3	0.000

distance b_0^* of the subcell and the distance s^* between two adjacent spots in a cluster (see Fig. 3d), the multiplicity could be calculated to be $m = b_0^*/s^*$. The average multiplicity value was calculated from a number of ED patterns of each sample. Some of the recorded patterns seemed to be commensurate, while others were incommensurate. The results in Table 1 show that the average m values obtained from the ED studies of the preparations are in agreement with those calculated from the XRPD data. The multiplicity decreases from $m = 13.5$ to $m = 11$ when the temperature is increased from 1000°C to 1350°C.

A large number of the ED patterns taken of thin crystallites from the low-temperature samples (E1–E6) were of the type shown in Fig. 4a. Diffuse streaking and weak superlattice reflections along the $\langle 100 \rangle$ directions of the pseudo-hexagonal subcell suggest frequent twinning of the structure. The corresponding HRTEM image (Fig. 4b), taken of a rather thick crystallite from the E2 sample, confirms that the crystal is disordered

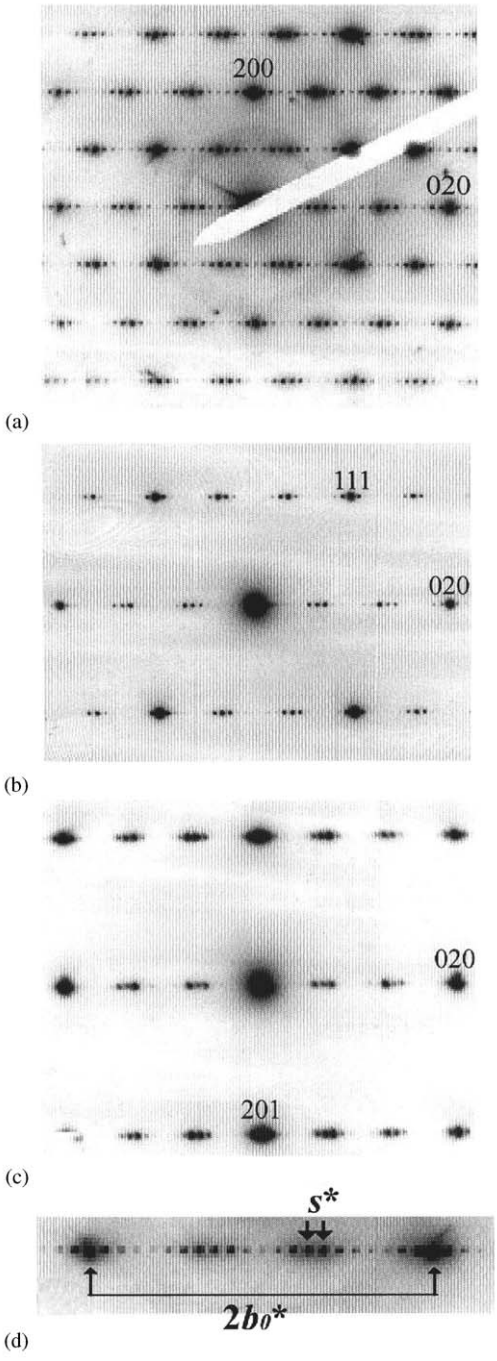

Fig. 3. Typical ED patterns taken from ordered crystallites aligned along: (a) [001], (b) [10−1], (c) [102], (d) an enlarged part of an array of $-1\,k\,0$ reflections from (a). The multiplicity ($m = b_0^*/s^*$) is calculated from the observed reflections.

and composed of three parts in twin orientations, marked A, B and C. The local average multiplicities calculated from parts A, B and C are 12.3, 12.7 and 12.3, respectively. These values are in fairly good agreement with the multiplicity $m = 13.1$ calculated from the corresponding ED pattern. The latter value is obtained from a larger part of the fragment, and the difference in m values might to some extent reflect the uncertainty in

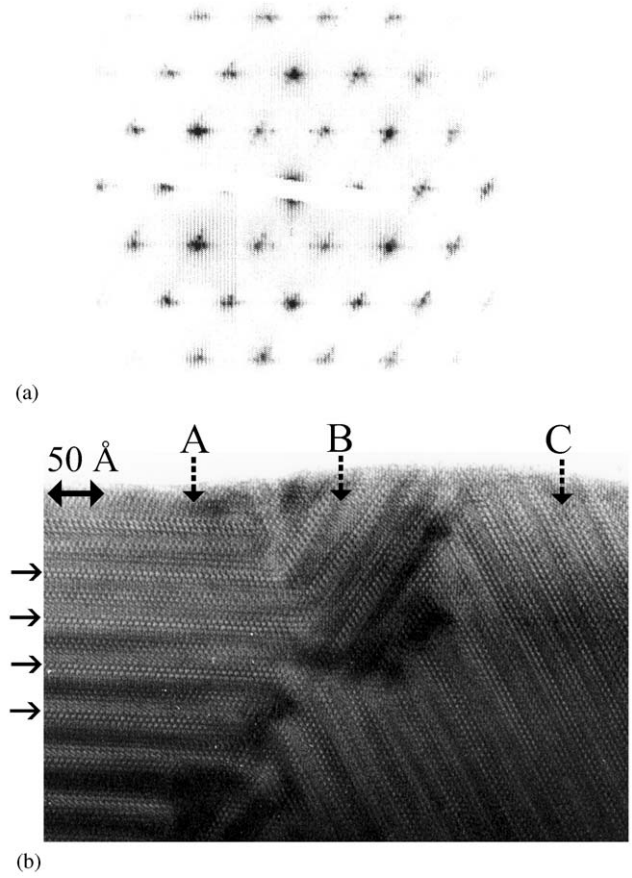

Fig. 4. (a) ED pattern taken of a crystallite from the E2 preparation ([001] zone). Streaking and superlattice reflections in twin orientations can be seen. (b) The corresponding HREM image shows three twin domains, marked A, B and C. The distance between two neighboring arrows to the left corresponds to the width of the L-Ta_2O_5 slab, from which the m value can be calculated.

the measurements. The arrows to the left in Fig. 4b show that the widths of the L-Ta_2O_5 slabs vary slightly. The dominating slab widths seem to correspond to $m = 12$ and 13, however. Each part of the crystallite can thus be considered as built up mainly by disordered intergrowth of L-Ta_2O_5 slabs with multiplicities of $m =$ 12 and 13.

The micrograph in Fig. 5 is taken in [001] projection from another L-Ta_2O_5 fragment of the E2 preparation. The m value was found to be $\approx$13.5 from the corresponding ED pattern. A contrast modulation with dark and bright bands perpendicular to b can be seen in the image. The distance between two neighboring dark bands illustrates the thickness of the corresponding L-Ta_2O_5 slab. By measuring the distances, the local multiplicity values were calculated. In the left part of the image, A, and also in the part marked B, the distance between the bands varies within the range $m =$ 12.6−13.5. In the middle of the image there is a small region where the two parts seem to overlap. Here the

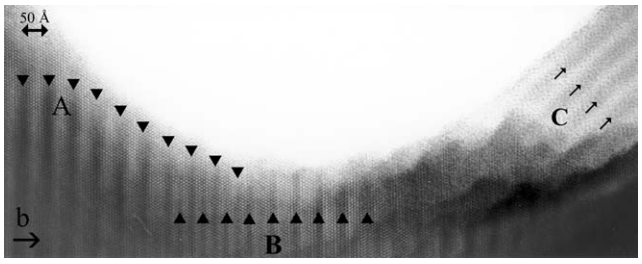

Fig. 5. HRTEM image of a crystallite from preparation E2 projected along [001]. Dark bands marked by arrows can be seen at A and B. The distance between neighboring arrows corresponds to the width of the L-Ta_2O_5 slab. The local m values were found to be in the range 12.6–13.5. A partly crystallized region is marked C.

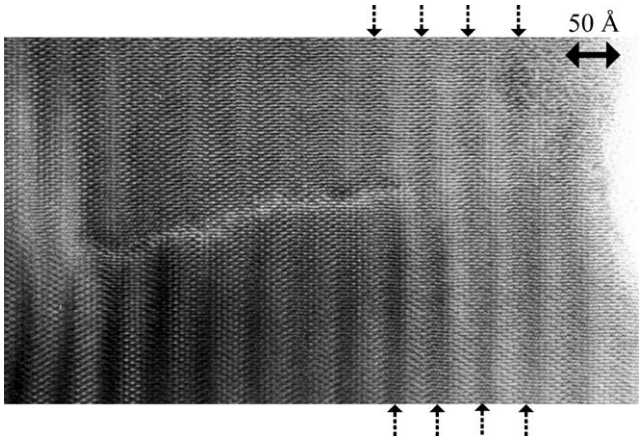

Fig. 6. HRTEM image of a thin crystallite ([001] zone) from the preparation E8.21, showing displacements of the L-Ta_2O_5 slabs across a fault boundary.

distance between the bands is about half of that in the rest of fragment. It seems likely, however, that the difference in contrast modulation between parts A and B is due to crystal tilt. Another reason might be that the L-Ta_2O_5 structure is just being formed, since the micrograph clearly shows crystallization of L-Ta_2O_5 from an amorphous state. In the right-hand part of the image, C, an amorphous region is linked to a fairly crystalline part, and the L-Ta_2O_5 type structure seems to be forming at the boundary. It is also noteworthy that the distances between the faint diffuse bands (see arrows at C) are about the same as those in the ordered parts of the crystallite. Several ED patterns typical of amorphous structures have been taken of fragments from the E2 sample. However, the number of crystallites with amorphous or twinned structures decreased in the samples, when the preparation temperature and the heating time were increased.

No crystal displaying twinning was seen in the samples (E8–E8.23) heated to 1300°C. The HRTEM examination of these crystallites revealed other defect types, such as cracks and fractures. The defect boundaries were usually fairly parallel to b, but a few fault planes at an angle of 30–60° to the b-axis were also seen. The HRTEM image in Fig. 6 is taken of a defect-rich L-Ta_2O_5 crystal from E8.21. The multiplicity of the crystal ($m \approx 12.2$) was calculated from the corresponding ED pattern. The defect region in the image shows that the dark and bright bands of different contrast features are displaced in relation to each other across the diffuse fault boundary. The average multiplicity value ($m \approx 11$) calculated from the top part is slightly less than that ($m \approx 11.9$) of the bottom region. The difference in width of the L-Ta_2O_5 slabs, and the observed difference in m values across the fault indicate that lateral ordering takes place in the L-Ta_2O_5 structure by small movements of atoms during the thermal treatment. The results show that the multiplicity value decreases towards $m = 11$, which apparently represents the stable low-temperature form of L-Ta_2O_5 at 1350°C.

Those preparations that had undergone long annealing at high temperatures gave definitely more ordered crystals. The HRTEM image in Fig. 7a is taken of a thin fragment from preparation E8.23. The corresponding ED pattern indicated an ordered modulated structure of multiplicity $m = 11$. Fig. 7b is obtained by crystallographic image processing of the HRTEM image by the CRISP program [29], and a model of a possible structure based on its contrast features is proposed in Fig. 7c. A structure determination of L-Ta_2O_5 ($m = 11$) from HRTEM images by crystallographic image processing in combination with a Rietveld X-ray powder diffraction refinement on the subcell will be published.

4. Discussion

The results shown in Fig. 2 and in Table 1 are obtained from as-received Ta_2O_5 and from specimens calcined in air at increasing temperatures, from 550°C up to 1350°C, for indicated periods of time. The densities range from 8.61 (at 850°C) to 8.79 g/cm^3 at 1340°C, thus increasing with increasing temperature of treatment. Comparing the densities of samples E8.22 and E8.23, it seems that longer heating times give denser structures. The values are well above those reported in Ref. [5,6] and somewhat below that given in Ref. [8]. It should be noted that the observed densities are higher than the calculated density of 8.31 g/cm^3 from a single-crystal structure determination of L-Ta_2O_5 [20]. It should further be noted that the calculated numbers of formula units, Z_{sub}, for all samples range from 1.038 to 1.058. This will be further commented upon below.

The multiplicities were calculated from q values [28], obtained from indexed X-ray powder diffraction patterns (XRDP), according to the formula $m = 1/(2-3q)$ as shown in Table 1. Multiplicity data from XRDP and the ED study are assumed to give an average value from

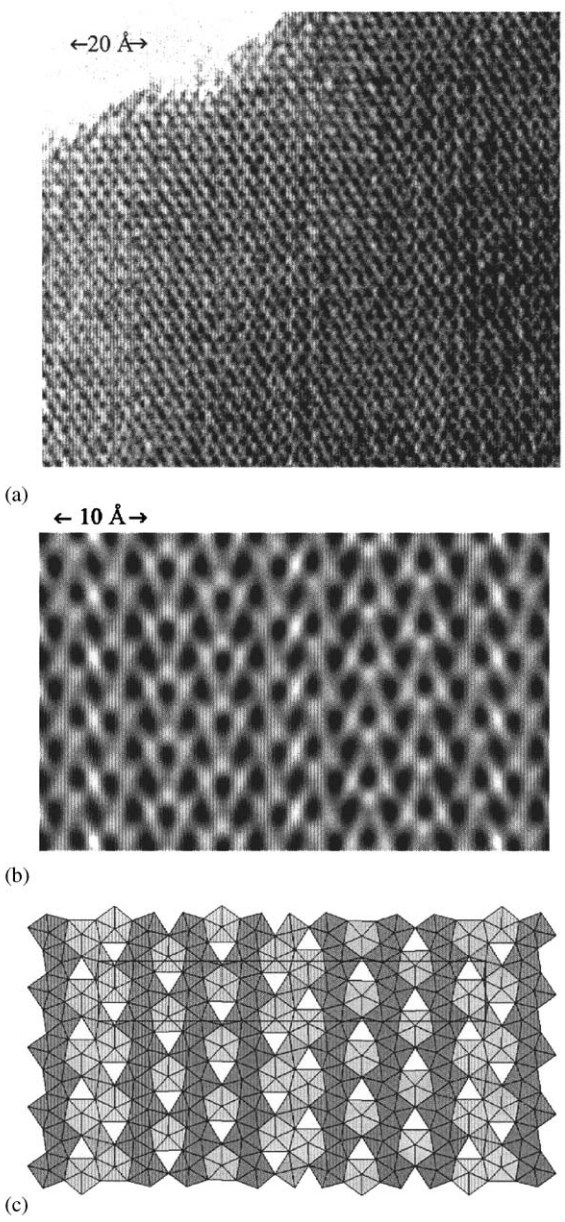

Fig. 7. (a) HRTEM image of a L-Ta_2O_5 crystal with $m = 11$ projected along the 3.9 Å axis. (b) The image processed by the CRISP program. (c) Structure model of L-Ta_2O_5 deduced form the processed image in (b). The interstitial Ta atoms in the three-sided tunnels are not drawn.

the actual sample, and the two sets of data agree in general. Table 1 shows a general decrease with increasing temperature of treatment for temperatures at 1000°C and above, with m values ranging from about 13.5 at 1000°C to 11.0 at 1350°C. This is in good agreement with earlier work (3, 10, 12, 13, 18), although the multiplicities given in Ref. [12] apparently have to be halved. It is notable that an L-Ta_2O_5 specimen held at high temperature and then annealed at 550°C preserves the multiplicity and the density acquired at the higher temperature, cf. samples E8 and E8.21 in Table 1, indicating that the annealing temperature is too low to bring about a noticeable change in the sample. On the other hand, experiments showed treatment of a high-temperature sample (E8) at 900°C for 3 weeks to result in m increasing from 12.6 to 13.6. No change in density was observed, however.

It was also found that treatment of E4 (annealed at 850°C) at the slightly higher temperature of 900°C for about three weeks resulted in a density increase from 8.61 to 8.71 g/cm^3. The multiplicity, however, was not changed. It thus appears that the multiplicity of L-Ta_2O_5 responds to changes in temperature irrespective of earlier heat treatments. It also seems that the observed density depends on the thermal pre-history of the sample in such a way that a density acquired at a high temperature cannot be changed by annealing at a lower temperature for reasonable periods of time. Our results also show that there are two stable low-temperature modifications of Ta_2O_5, one below 1000°C ($m \approx 13.5$) and the other at 1350°C ($m = 11$), thus generally confirming earlier results [3,10,22]. However, electron microscopy studies show that local variations of multiplicity values are abundant, indicating a high degree of disorder in the L-Ta_2O_5 structure.

With the results obtained we may now estimate the number of atoms in L-Ta_2O_5 of a given multiplicity. For an L-Ta_2O_5 specimen heated at 1350°C (E8.22 in Table 1) we find $Z_{sub} = 1.052$, giving a calculated cell content of $Ta_{23.144}O_{57.860}$ or $Ta_{23.2}O_{58}$ for an 11-fold superstructure. Similarly, we obtain for L-Ta_2O_5 heated at 1000°C (E5 in Table 1) $Z_{sub} = 1.046$ giving $Ta_{27.196}O_{67.990}$ or $Ta_{27.2}O_{68}$ for a 13-fold superstructure. A 14-fold superstructure gives $Ta_{29.29}O_{73.22}$, or $Ta_{29.6}O_{74}$. Density measurements indicate, assuming the occurrence of 11- and 13- (or 14)-fold superstructures without oxygen vacancies, that there are 1.2–1.6 extra, interstitial, Ta atoms per unit cell in these two samples.

In this connection it is interesting to note Lehovec's comments on the structure of L-Ta_2O_5. He assumed a possible "incorporation of foreign ions, particularly cations" into the plane of apical oxygens at $z = 1/2$ [5]. It is also interesting to note that in their structure determination of L-Ta_2O_5 with $m = 11$, Stephenson and Roth discussed an ideal model with 58 oxygens in the unit cell [20]. Assuming 22 Ta atoms in the cell they had to introduce oxygen vacancies in so-called distortion planes in the structure, whereby the number of oxygens was reduced to 55. Our density measurements do not contradict an ideal model with 58 oxygen and 22 tantalum atoms per cell, as suggested in Ref. [20], but with additional Ta atoms interstitially inserted to achieve electroneutrality. This is also in line with the findings of Harburn et al. [27].

The new proposed crystal structure of L-Ta_2O_5 with $m = 11$ in Fig. 7c is in agreement with the conclusions reached above. The model can be described as an

ordered intergrowth of slabs of α-U_3O_8 and β-U_3O_8 type. The α-U_3O_8 slabs are built up entirely from pentagonal TaO_7 bipyramids linked by corner- and edge-sharing so that tunnels with three-sided passages are created. These slabs constitute the major part of the structure. Their composition corresponds to Ta_3O_8. The β-U_3O_8 slabs, the minor part, consist of pentagonal TaO_7 bipyramids and TaO_6 octahedra in a corner- and edge-sharing arrangement. The passages of the resulting tunnels are narrower than those of α-U_3O_8 type. The width of these slabs is such that the composition corresponds to Ta_2O_5. The α-U_3O_8 slabs (of Ta_3O_8 stoichiometry) with their somewhat wider tunnels thus appear to be more suitable for interstitial Ta atoms than the slabs of β-U_3O_8 type (with Ta_2O_5 stoichiometry), resulting in tricapped trigonal prismatic coordination, for example as in $K_6Ta_{10.8}O_{30}$ [32]. It is of course still possible that L-Ta_2O_5 contains some oxygen vacancies, but the occurrence might be lower than hitherto thought. In the L-Ta_2O_5-type structures of $Ta_{74}W_6O_{203}$ (Fig. 1b) and $Ta_{22}W_4O_{67}$ (Fig. 1c), on the other hand, the β-U_3O_8 type slabs comprise the major part of the structure. The reason might be that the tungsten atoms prefer octahedral coordination, present in the β-U_3O_8 type slabs [25].

Acknowledgments

We wish to thank Jaroslava Östberg for technical assistance with the photographic work. Financial support from The Swedish Research Council is gratefully acknowledged.

References

[1] S. Lagergren, A. Magnéli, Acta Chem. Scand. 6 (1952) 444.
[2] A. Reisman, F. Holtzberg, M. Berkenblit, M. Berry, J. Am. Chem. Soc. 78 (1956) 4514.
[3] R.S. Roth, J.L. Waring, J. Res. Natl. Bur. Stand. Sect. A 74 (1970) 485.
[4] G. Harburn, R.J.D. Tilley, R.P. Williams, Philos. Mag. A 68 (1993) 633.
[5] K. Lehovec, J. Less-Common Met. 7 (1964) 397.
[6] A. Reisman, F. Holtzberg, in: A.M. Alper (Ed.), High Temperature Oxides II, Academic Press, New York, London, 1970, p. 217.
[7] L. Frevel, H. Rinn, Anal. Chem. 27 (1955) 1329.
[8] N. Terao, J. Appl. Phys. Tokyo 6 (1967) 21.
[9] R. Moser, Schweiz. Mineral. Petrogr. Mitt. 45 (1965) 35.
[10] R.S. Roth, J.L. Waring, H.S. Parker, J. Solid State Chem. 2 (1970) 445.
[11] J.L. Waring, R.S. Roth, J. Res. Natl. Bur. Stand. Sect. A 72 (1968) 175.
[12] J.M. Williams, R.J.D. Tilley, G. Harburn, R.P. Williams, J. Solid State Chem. 92 (1991) 460.
[13] R.S. Roth, N.C. Stephenson, in: L. Eyring, M. O'Keefe (Eds.), Chemistry of Extended Defects in Non Metallic Solids, North-Holland, Holland, Amsterdam, 1970, p. 117.
[14] N.C. Stephenson, R.S. Roth, Acta Crystallogr. B 27 (1971) 1010.
[15] N.C. Stephenson, R.S. Roth, Acta Crystallogr. B 27 (1971) 1018.
[16] N.C. Stephenson, R.S. Roth, Acta Crystallogr. B 27 (1971) 1031.
[17] T. Miyano, K. Kosuge, Eur. J. Solid State Inorg. Chem. 31 (1994) 867.
[18] T. Miyano, J. Solid State Chem. 126 (1996) 208.
[19] T. Miyano, Jap. Soc. Electron Microsc. 47 (1998) 47.
[20] N.C. Stephenson, R.S. Roth, Acta Crystallogr. B 27 (1971) 1037.
[21] A.F. Andresen, Acta Crystallogr. 11 (1958) 612.
[22] T.R. Wagner, J. Solid. State Chem. 91 (1991) 189.
[23] H.-U. Hummel, R. Fackler, P. Remmert, Chem. Ber. 125 (1992) 551.
[24] S. Schmid, R.L. Withers, J.G. Thompson, J. Solid State Chem. 99 (1992) 226.
[25] S. Schmid, J.G. Thompson, A.D. Rae, B.D. Butler, R.L. Withers, N. Ishizawa, S. Kishimoto, Acta Crystallogr. B 51 (1995) 698.
[26] A.D. Rae, S. Schmid, J.G. Thompson, R.L. Withers, N. Ishizawa, Acta Crystallogr. B 51 (1995) 709.
[27] G. Harburn, R.J.D. Tilley, J.M. Williams, R.P. Williams, J. Hutchison, J. Chem. Soc. Faraday Trans. 88 (1992) 621.
[28] B.-O. Marinder, J. Solid State Chem. 160 (2001) 62.
[29] S. Hovmöller, Ultramicroscopy 41 (1992) 121.
[30] J. Harvey, H. Wilman, Acta Crystallogr. 14 (1961) 1278.
[31] J. Spyridelis, P. Delavignette, S. Amelinckx, Phys. Status Solidi 19 (1967) 683.
[32] A.A. Awadalla, B.M. Gatehouse, J. Solid State Chem. 23 (1978) 349.